

PAPER • OPEN ACCESS

Elastic temporal waveguiding

To cite this article: Jonatha Santini and Emanuele Riva 2023 *New J. Phys.* **25** 013031



View the [article online](#) for updates and enhancements.

You may also like

- [Transferring orbital and spin angular momenta of light to atoms](#)
A Picón, A Benseny, J Mompart et al.
- [Tractable calculation of the Green's tensor for shear wave propagation in an incompressible, transversely isotropic material](#)
Ned C Rouze, Mark L Palmeri and Kathryn R Nightingale
- [Two-dimensional spatiotemporal pattern formation in the double barrier resonant tunnelling diode](#)
G Stegemann and E Schöll



PAPER

Elastic temporal waveguidingJonatha Santini  and Emanuele Riva* 

Department of Mechanical Engineering, Politecnico di Milano, Milano 20156, Italy

* Author to whom any correspondence should be addressed.

E-mail: emanuele.riva@polimi.it**Keywords:** time modulation, waveguiding, frequency conversion, adiabatic theorem, metamaterials, phononic crystals, scatteringSupplementary material for this article is available [online](#)

OPEN ACCESS

RECEIVED
15 July 2022REVISED
14 January 2023ACCEPTED FOR PUBLICATION
18 January 2023PUBLISHED
1 February 2023Original Content from
this work may be used
under the terms of the
[Creative Commons
Attribution 4.0 licence](#).Any further distribution
of this work must
maintain attribution to
the author(s) and the title
of the work, journal
citation and DOI.**Abstract**

We provide a theoretical framework to mold time-modulated mechanical metamaterials with frequency conversion and wave-steering capabilities. To illustrate the concept, we initially focus on 1D lattices, whereby a sufficiently slow time-modulation of the stiffness is employed to convert the frequency content of impinging waves. Based on the adiabatic theorem, we demonstrate that undesired reflections, which emerge in time-discontinuous materials, can be dramatically reduced by a careful choice of the modulation velocity. The concept is later explored in the context of 2D lattices, whereby a slow time modulation of the stiffness not only induces frequency conversion with minimal back-scattering, but also serves as a mechanism to steer waves. Our paper explores a new and exciting way to control wave propagation in elastodynamics with scattering-free guiding capabilities, and may open new avenues for the manipulation and transport of information through elastic waves.

1. Introduction

The dynamics of space, time, and space-time tessellated materials is nowadays explored in several realms of physics to promote rich and unprecedented phenomena not naturally observable. In the context of elastodynamics, materials dressed with space, time, and space-time modulations are conveniently molded to manipulate wave motion at will. Examples have shown different forms of waveguiding that rely on defect mechanisms [1], topological insulators [2–12], metagradings [13–21], transformation optics and acoustics [22–32], which are passive strategies effectively employed to accomplish relevant technological behaviors, such as communication, focusing, and invisibility.

To enrich the dynamical landscape of today, exotic functionalities can be sought by accessing the temporal degree of freedom, which consists of time-varying materials that usually require feeding additional energy into otherwise passive systems. The activation of time-dependent interactions has recently revealed new physics, including studies on unidirectional waves [33–37], adiabatic pumping [38–42], frequency conversion [43], and parametric amplification [44].

All examples above are induced either by space or time heterogeneity, whereby each discontinuity is capable of generating wave scattering, incremental steering, pumping, or asymmetry, depending on the steepness of the discontinuity. Spatial modulations obey Snell's law, yielding a frequency-invariant wavenumber transformation across the discontinuities. In contrast, a temporal version of Snell's law requires the transformation to occur at constant wavenumber while varying the frequency across the time discontinuity [45]. The complex interplay between consecutive space, time, and space-time modulations, can generate scattering patterns with attenuation, amplification, nonreciprocity, or waveguiding capabilities observable in metamaterials and phononic systems. Even though the implementation of space-time and time-discontinuous materials can be challenging, the efforts done in this direction have led to experimental papers which have propelled the research done in the field of active phononics [46, 47].

In this paper, we focus our attention on time-discontinuous 1D and 2D lattices as a reference example. Within this framework, a general procedure for the analysis of wave motion of arbitrary time-varying mechanical systems is illustrated, which is functional for temporal waveguiding, wave steering and frequency conversion. Practically, we show how the time-modulation parameters are linked to the frequency conversion/wave steering capabilities.

Motivated by prior works on materials with time-varying permittivity [45, 48], we initially pursue frequency conversion in 1D elastic lattices via adiabatic stiffness-modulation. In contrast to [45], a smooth time-modulations is herein applied to a dispersive elastic medium, whereby the gradual variation of the stiffness is key in avoiding undesired reflections during the frequency transformation of propagating wave-modes (i.e. the states that populate the lattice). The adiabatic theorem is employed to grasp the implied scattering phenomena emerging in arbitrary continuous modulations, and allows us to provide a connection between the modulation velocity and the energy leak between all states that populate the lattice, i.e. in the case at hand, two counter-propagating waves.

In analogy to [48], this concept is also explored in 2D time-modulated lattices, where the frequency conversion is accompanied by a temporal curvature of wave motion. Differently to [48], we employ a smoothly varying time-dependent stiffness instead of a fast isotropic-to-anisotropic modulation protocol, and we discuss the role of the velocity of modulation on the nucleation of back-scattered waves and steering performance. We show how this concept can be engineered to produce scattering-free waveguides capable of sending an elastic wave packet between an emitter and a receiver in a controllable manner.

The procedure employed herein is general and applicable to more complex scenarios, such as elastic waves in the continuum, in multi-physics materials, and in more complex metamaterial systems characterized by dispersion relations with a remarkable degree of controllability. Our paper explores a new way to manipulate wave motion which may promote additional efforts in the context of time-modulated materials.

2. Frequency conversion in stiffness-modulated 1D lattices

We start the discussion by considering the spring-mass system displayed in figure 1(a). As mentioned, scope of this section is to perform frequency conversion in such a system with minimal nucleation of back-scattered waves. We remark that time-modulated materials are known to exhibit frequency conversion and we hereafter present a simple and viable way to pursue this scope. As such, our lattice is made by a number $N = 300$ of unitary masses $m = 1$, separated by unitary distance $d = 1$, and linked by springs which embody time-varying characteristics $k(t)$. Without any loss of generality, we focus our attention on linear time-modulation laws, but different functions can be employed:

$$k(t) = k_i + v(t - t_i) \quad (1)$$

here, $v = (k_f - k_i) / (t_f - t_i)$ is the modulation speed, which is a fundamental parameter for frequency conversion and allows for controlling the scattering phenomena within the modulated material. $k_i = 1$ and $k_f = 0.2$ are the initial and final values for the stiffness, t_i is the activation time instant for $k(t)$ and t_f is the final time of the modulation. The key idea is elucidated in figure 1(b): when a wave impinges across a temporal discontinuity, a pair of counter-propagating waves are generated, whose magnitude depends on the adiabaticity of the temporal transformation and the stiffness-modulation levels. We hereafter provide a qualitative condition that links the reflection and transmission characteristics of the time interface to the velocity of the modulation v . To that end, we follow and adapt the derivation detailed in our prior works, and we make it applicable to handle wave propagation problems [38, 41].

First and foremost, the procedure requires the elastodynamic equation to be expressed by way of a first-order differential form akin to the Schrödinger equation. We start the derivation from the second order differential form:

$$m\ddot{u}_n + 2ku_n - k(u_{n+1} + u_{n-1}) = 0 \quad (2)$$

where $u_n = u_n(t)$ describes the longitudinal motion of the n th mass and, to ease notation, the time dependence of k is implicitly assumed. In the attempt to study the coupling between counter propagating wave modes, we focus on time-dependent dispersion properties of the lattice, which obey the unit cell dynamics with implied Floquet-Bloch conditions. Hence, Ansatz u_n are expressed in the complex exponential form $u_n = \hat{u}_n e^{i\mu n}$, where $\mu = \kappa d$ is the dimensionless wavenumber. After substitution into equation (2), the relevant dynamic equation takes the following convenient form:

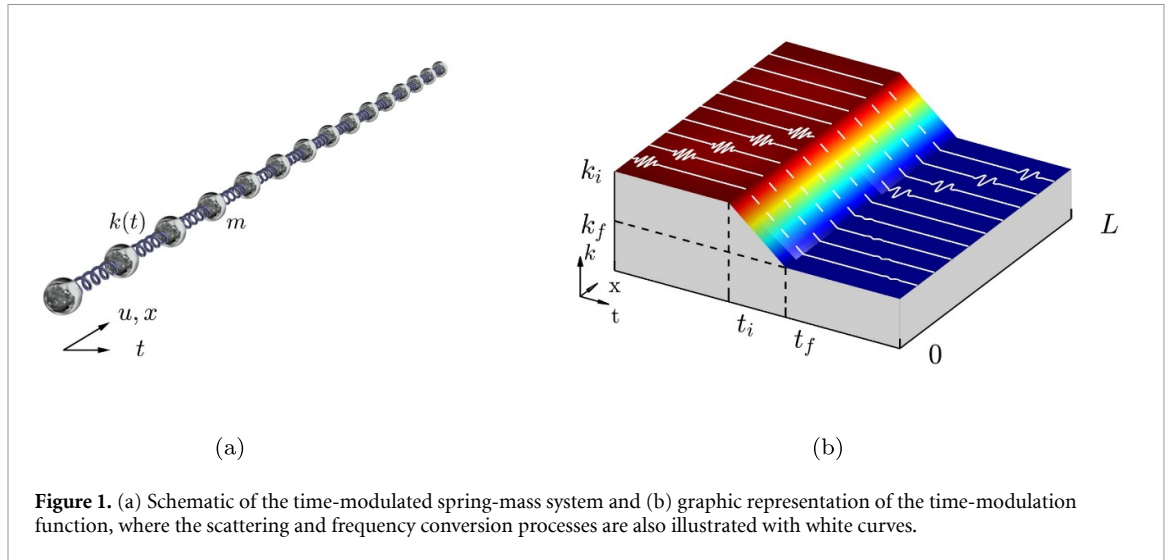


Figure 1. (a) Schematic of the time-modulated spring-mass system and (b) graphic representation of the time-modulation function, where the scattering and frequency conversion processes are also illustrated with white curves.

$$|\hat{\Psi}_{n,t}\rangle = H(\mu, t) |\hat{\Psi}_n\rangle \quad |\hat{\Psi}_n\rangle = \begin{pmatrix} \hat{p}_n \\ \hat{u}_n \end{pmatrix} \quad H(\mu, t) = \begin{bmatrix} 0 & -2k(1 - \cos\mu) \\ \frac{1}{m} & 0 \end{bmatrix} \quad (3)$$

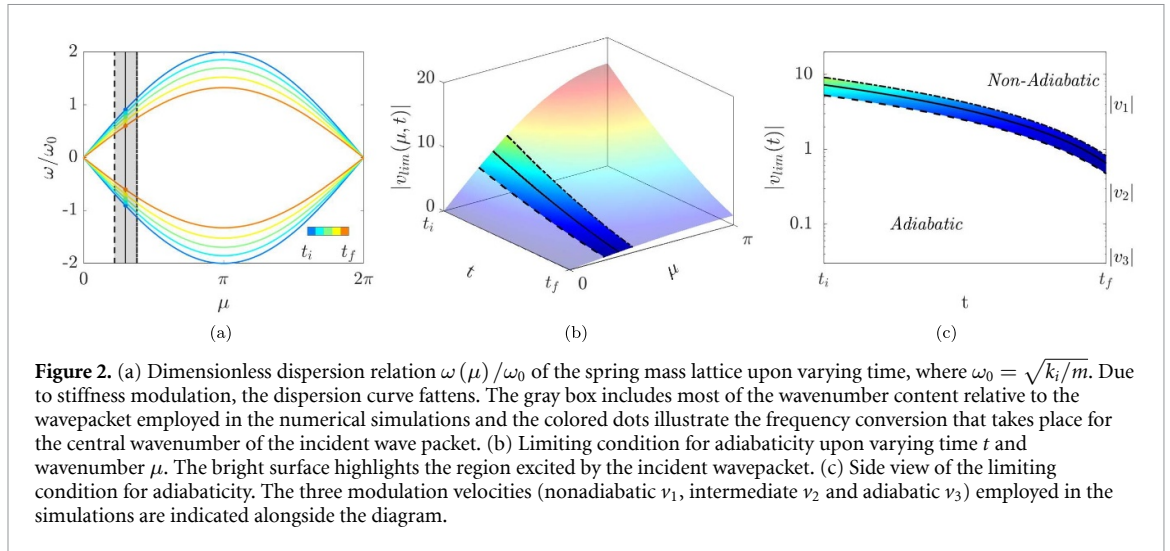
where $\hat{p}_n = m\hat{u}_{n,t}$ is the linear momentum and $H(\mu, t)$ is the 2×2 time-dependent dynamical matrix with incident wavenumber μ . We note that any incident wave packet can be written as a linear combination of $2M + 1$ plane waves in Fourier space $|\Psi_n\rangle = \sum_{m=-M}^M |\hat{\Psi}_n(\mu_m)\rangle e^{i\mu_m x}$, where $\mu_m = m \frac{2\pi}{Nd}$ are the impinging wavenumbers considered in the expansion and $|\hat{\Psi}_n(\mu_m)\rangle$ are the associated amplitude coefficients accommodating momentum and displacement. Hence, equation (3) suitably describes the evolution of the amplitude coefficient $|\hat{\Psi}_n(\mu_m)\rangle$ for wave packets $|\Psi_n\rangle$ propagating through the time-modulated lattice, when the arbitrary incident wavenumber for a single plane wave μ is replaced by μ_m and $2M + 1$ dynamic equations for $|\hat{\Psi}_n(\mu_m)\rangle$ are considered. Due to a temporal version of Snell's law [45], the impinging wavenumbers are invariant during time integration, whereby the initial conditions for $|\hat{\Psi}_n(\mu_m)\rangle$ can be regarded as the amplitude coefficients for the incident wave packet in momentum space. Such coefficients evolve in time differently for different wavenumbers, both in terms of amplitude and frequency. This aspect plays a role in the adiabaticity of the transformation and, hence, will be hereafter discussed more in depth.

To shed light on this matter, we consider a waveguide with a quasi-static variation of the properties, i.e. whose modulation velocity is much slower than the time-scale of the underlying dynamics, whereby the solution can be synthesized in a complex exponential form $|\hat{\Psi}_n(\mu_m)\rangle = |\psi^R(\mu_m)\rangle e^{j\omega(\mu_m)t}$. As such, for a single incident wavenumber μ_m , the system supports a pair of states $\omega_{1,2} = \pm\omega$ that instantaneously populate the waveguide at time t and are dictated by the right eigenvalue problem $H(\mu_m, t) |\psi_h^R\rangle = j\omega_h |\psi_h^R\rangle$. Such states correspond to counter-propagating waves whose frequencies are illustrated through the dispersion relations in figure 2(a). To ease notation, the wavenumber dependence $|\psi_h^R\rangle = |\psi_h^R(\mu_m)\rangle$ and $\omega_h = \omega_h(\mu_m)$ is implicitly assumed in what follows.

Now, when the temporal modulation is sufficiently slow, a quasi-static evolution takes place such that the impinging wave, either at ω_1 or at ω_2 , is frequency-converted consistently to the time-evolution of the dispersion relation marked with colored dots. We remark that a single value for μ_m is assumed, corresponding to a right-traveling plane wave with unitary amplitude coefficient $|\hat{\Psi}_n\rangle = |\psi_1^R\rangle e^{j\omega_1 t}$ as initial condition at $t = 0$, where $|\psi_1^R\rangle$ is the right eigenvector relative to ω_1 . During time modulation, the solution is synthesized as a linear combination of the two states supported by the waveguide $|\hat{\Psi}_n\rangle = \sum_{h=1}^2 a_h |\psi_h^R\rangle e^{j\theta_h}$, weighted by participation factors a_h , where $\theta_h = \int_0^t \omega_h(\tau) d\tau$. In other words, if some energy is present in one state, say $\omega_1 = +\omega$, a part of that can leak to $\omega_2 = -\omega$, depending on the time-modulation parameters. Time evolution for the r^{th} participation factor a_r with $r = 1, 2$ is dictated by the following equation (see appendix for the derivation):

$$a_{r,t} = -\langle \psi_r^L | \psi_{h,t}^R \rangle a_r - \sum_{h \neq r} \frac{\langle \psi_r^L | H(\mu_m, t) | \psi_h^R \rangle}{j(\omega_h - \omega_r)} a_h e^{j(\theta_h - \theta_r)}. \quad (4)$$

Note that all quantities present in equation (4) are wavenumber-dependent and, hence, different incident wavenumbers will produce a different dynamic evolution for the coefficients a_h . As a result, the wavefield will be populated by reflected and transmitted wavepackets and will be a combination of terms



$|\Psi_n\rangle = \sum_{m=-M}^M |\hat{\Psi}_n(\mu_m)\rangle e^{jn\mu_m}$ where $|\hat{\Psi}_n(\mu_m)\rangle = \sum_{h=1}^2 a_h(\mu_m) |\psi_h^R(\mu_m)\rangle e^{j\theta_h(\mu_m)}$. Since $|\psi_h^R(\mu_m)\rangle$, $\langle \psi_h^L(\mu_m) |$, $\theta_h(\mu_m)$, $H(\mu_m),_t$, $a_h(\mu_m)$ evolve differently for different μ_m values, the incident wavepacket will be moderately distorted by time modulation. In addition, we note that the second term into equation (4) is responsible for the energy leak between the two states, whereby only if $H_{,t} = 0$ the dynamic equations for the participation factors a_r are uncoupled. By further manipulating equation (4), and following the procedure described in [38, 41], we get to a limiting condition for adiabaticity (appendix):

$$\left| \frac{\langle \psi_2^L | H(\mu_m, t),_t | \psi_1^R \rangle}{(\omega_2 - \omega_1)^2} \right| \ll 1 \tag{5}$$

which is a condition for the modulation to provide negligible energy transfer from state 1 to state 2 and is valid for any incident wavenumber μ_m . In order for the expression to apply, the left and right eigenvectors $\langle \psi_{1,2}^L |$ and $|\psi_{1,2}^R\rangle$ are normalized such that $\langle \psi_s^L | \psi_r^R \rangle = \delta_{sr}$. The analytical expressions for the eigenstates are:

$$\begin{aligned} \omega_{1,2} &= \pm \sqrt{\frac{2k(\cos \mu - 1)}{m}} && \text{with:} \\ |\psi_1^R\rangle &= \begin{pmatrix} j\sqrt{mk(\cos \mu - 1)} \\ \frac{\sqrt{2}}{2} \end{pmatrix} && \langle \psi_1^L | = \begin{pmatrix} 1 \\ j\sqrt{4mk(\cos \mu - 1)} \quad \frac{\sqrt{2}}{2} \end{pmatrix} \\ |\psi_2^R\rangle &= \begin{pmatrix} -j\sqrt{mk(\cos \mu - 1)} \\ \frac{\sqrt{2}}{2} \end{pmatrix} && \langle \psi_2^L | = \begin{pmatrix} 1 \\ -j\sqrt{4mk(\cos \mu - 1)} \quad \frac{\sqrt{2}}{2} \end{pmatrix} \end{aligned} \tag{6}$$

where the above quantities are expressed again for arbitrary values of μ . Merging equations (5) and (6), we get to a limiting condition for the rate of change v , in order for the modulation to induce an adiabatic transformation to the incident state:

$$|v_{\text{lim}}| \ll 16 \left| \sin \frac{\mu}{2} \right| \sqrt{\frac{k^3}{m}} \tag{7}$$

which is function of both incident wavenumber μ and time t . This condition is mapped in figure 2(b), where the region including most of the incident wavenumber content, and hereafter employed for simulations, is highlighted. Hence, figure 2(b) is suitable for qualifying the adiabaticity of non-monochromatic wave packets. That is, when the limiting condition is satisfied for the incident wavenumber content, the transformation can be considered adiabatic.

We now perform numerical simulations to qualify the dynamic behavior discussed above, and in the attempt to capture limiting conditions expressed in equation (7). The values employed in the simulations are $v_1 = -3.5$, $v_2 = -0.23$ and $v_3 = -0.03$, which are represented in figure 2(c) and superimposed to the lateral view of figure 2(b). These values correspond to a nonadiabatic, intermediate, and adiabatic modulation speeds for the entire incident wavenumber spectrum from t_i to t_f .

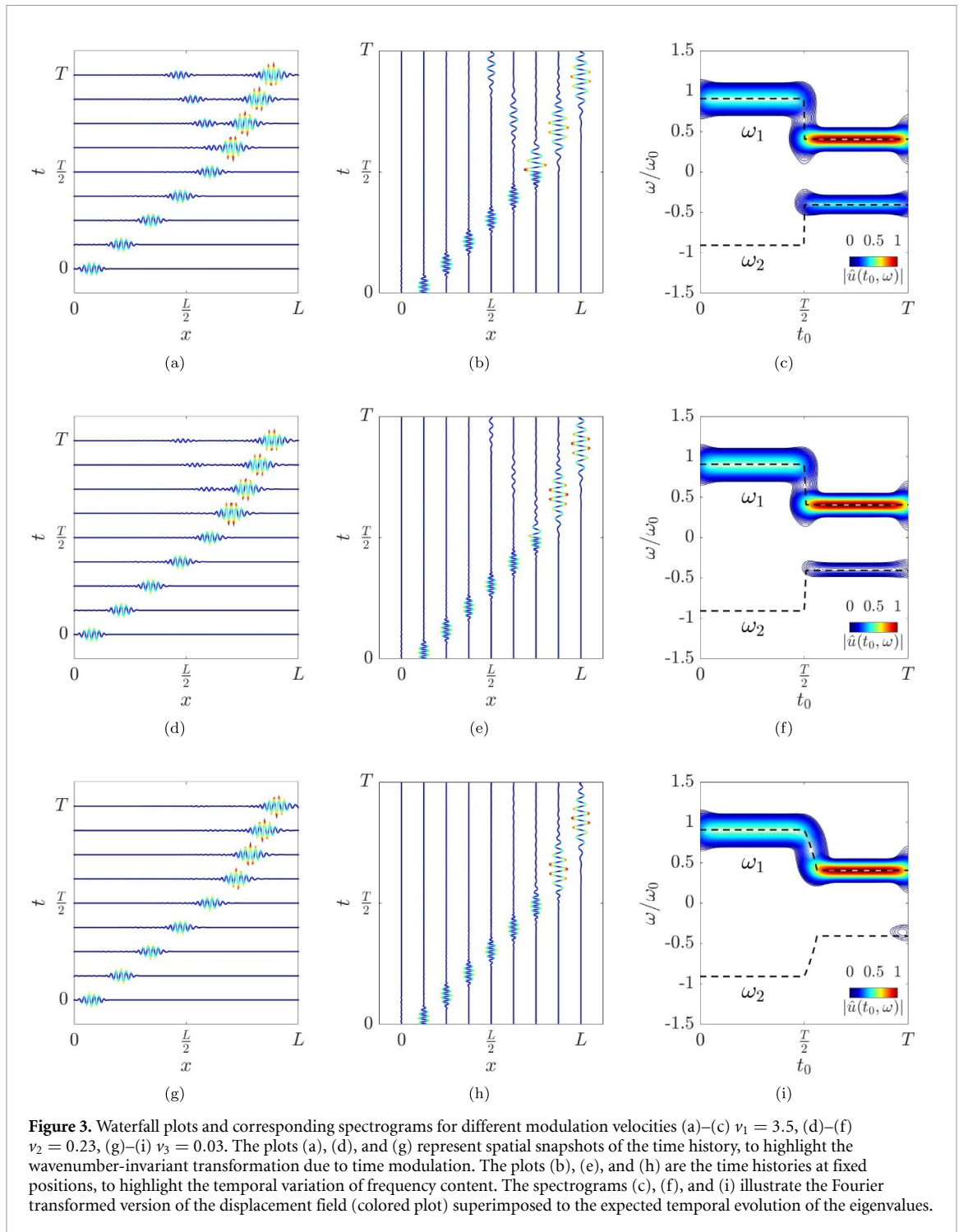


Figure 3 illustrates results for an impinging Gaussian wavepacket with number of periods $n = 10$ and central wavenumber $\mu = 0.3\pi$, which is provided as initial condition for the simulations. The time histories are conveniently represented with space-time diagrams in figures 3(a)–(b), (d)–(e), and (g)–(h) from $t = 0$ to $t = T$. Specifically, figures 3(a), (d) and (g) illustrate a wavenumber-invariant transformation, whereby the fixed-time displacement of the wave does not change shape during time modulation. In contrast, figures 3(b), (e) and (h) suitably represent the frequency change dictated by time-modulation, whereby the temporal period of the wave packet is clearly increased during modulation. Further relevant comments follow: (a) the wave packet decelerates during the transformation, consistently with the dispersion properties displayed in figure 2(a). (b) The frequency and velocity changes are accompanied by reflection and transmission of the impinging wave, whose magnitudes are dependent upon the modulation speed. The scattering level is reduced for lower velocity values v and eventually eliminated in case of purely adiabatic modulations.

This concept is better described by way of figures 3(c), (f) and (i), where the energy content within the waveguide (colored contours) is superimposed to the expected evolution of the states (dashed lines). Such spectrograms are herein evaluated by windowing the time history $u(x_n, t)$ through a moving Gaussian function $G = e^{-(t-t_0)^2/2c^2}$, where the parameter $c = T/20$ controls the width of the window and t_0 is smoothly varied between $t_0 \in [0, T]$, to capture the variation of the spectral content in time. The Fourier transformed version of the windowed displacement field $\hat{u}(t_0, \omega, \mu)$ is further post-processed by taking the L^2 norm in wavenumber space limited to $\mu > 0$, in order to eliminate one dimension and get to the convenient form $\hat{u}(t_0, \omega)$. In the figures, the energy is initially stored in the state $\omega_1 = +\omega$. After the modulation takes place, a certain amount of energy is scattered toward backward propagating states, i.e. in correspondence of $\omega_2 = -\omega$. This energy leak is observable in figure 3(c) and in figure 3(f) with minor intensity. In contrast, the configuration displayed in figure 3(i) exhibits a clear frequency conversion with negligible back-scattering, whereby all the energy remains confined in correspondence of $\omega_1 = \omega$, and the transformation can be considered adiabatic.

3. Temporal steering in stiffness-modulated 2D lattices

The discussion is now focused on the elastic lattice displayed in figure 4(a), which is made of 60×60 masses equally spaced by the lattice constant d , and connected to the nearest neighbors through linear springs k_x and k_y . For simplicity and without any loss of generality, $k_y(t)$ accommodates the temporal degree of freedom. By following the same line of work, we consider a linear time varying function for $k_y(t) = k_{yi} + \nu(t - t_i)$, capable of driving the stiffness value from k_{yi} to k_{yf} in a time interval $\Delta t = t_f - t_i$ with modulation velocity ν . The concept is elucidated in figure 4(b): an impinging wave that propagates across a temporal discontinuity experiences a frequency transformation and, provided that the modulation is adiabatic, the process occurs with negligible energy leak toward the back-propagating state. We hereafter demonstrate that such a frequency transformation is accompanied by a time-dependent curvature of wave motion, which serves as a mechanism to functionally control and guide waves.

We start the analysis from the time-dependent elastodynamic equation, which describes out-of-plane motion of the mass element sitting in position $\mathbf{r} = (n, m)$:

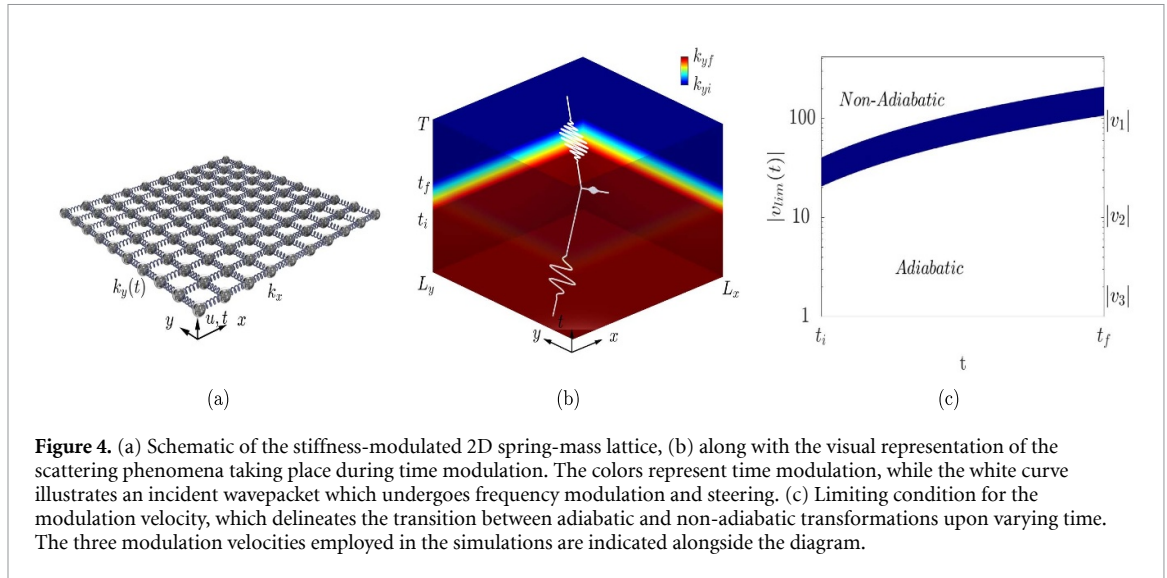
$$m\ddot{u}_{n,m} + 2(k_x + k_y)u_{n,m} - k_x(u_{n+1,m} + u_{n-1,m}) - k_y(u_{n,m+1} + u_{n,m-1}) = 0 \quad (8)$$

where to ease notation, the time dependence of $k_y(t)$ is implicitly assumed. Note that this system is fundamentally different than the one employed in [48], as the discrete nature of the system implies anisotropic and dispersive characteristics of wave motion. Now, wave propagation in such a system is investigated via a dispersion analysis of the unit cell with implied Floquet-Bloch boundary conditions, whereby the displacement $u_{n,m}(t)$ is described via complex exponential functions $u_{n,m} = \hat{u}e^{i\boldsymbol{\mu}\cdot\mathbf{r}}$, where $\boldsymbol{\mu} = (\mu_x, \mu_y)$ is the dimensionless wavevector. After a few mathematical steps we get to the following form:

$$|\hat{\Psi}\rangle, t = H(\boldsymbol{\mu}, t)|\hat{\Psi}\rangle \quad |\hat{\Psi}\rangle = \begin{pmatrix} \hat{p} \\ \hat{u} \end{pmatrix} \quad H(\boldsymbol{\mu}, t) = \begin{bmatrix} 0 & -2[k_x(1 - \cos \mu_x) + k_y(1 - \cos \mu_y)] \\ \frac{1}{m} & 0 \end{bmatrix} \quad (9)$$

which provide suitable description of the quasi-static evolution of two propagating eigenstates relative to an impinging wave $|\hat{\Psi}\rangle = |\Psi_h^R\rangle e^{i\omega_h t}$ with wavevector $\boldsymbol{\mu}$. At this point we would like to remark that the form in equation (9) is general and can be applied to a wide class of mechanical systems that can be approximated in terms of reduced mass and stiffness matrices with implied periodic conditions. Hence, the considerations hereafter presented and discussed above can thus be easily extended to many other examples. The eigenstates, solution of the quasi-static eigenvalue problem $H(\boldsymbol{\mu}, t)|\Psi_h^R\rangle = j\omega_h|\Psi_h^R\rangle$ are:

$$\begin{aligned} \omega_{1,2} &= \pm \sqrt{\frac{2}{m}(k_x(1 - \cos \mu_x) + k_y(1 - \cos \mu_y))} \\ |\psi_1^R\rangle &= \begin{pmatrix} j\sqrt{m(k_x(\cos \mu_x - 1) + k_y(\cos \mu_y - 1))} \\ \frac{\sqrt{2}}{2} \end{pmatrix} & \langle \psi_1^L | &= \left(\frac{1}{j\sqrt{4m(k_x(\cos \mu_x - 1) + k_y(\cos \mu_y - 1))}} \quad \frac{\sqrt{2}}{2} \right) \\ |\psi_2^R\rangle &= \begin{pmatrix} -j\sqrt{m(k_x(\cos \mu_x - 1) + k_y(\cos \mu_y - 1))} \\ \frac{\sqrt{2}}{2} \end{pmatrix} & \langle \psi_2^L | &= \left(-\frac{1}{j\sqrt{4m(k_x(\cos \mu_x - 1) + k_y(\cos \mu_y - 1))}} \quad \frac{\sqrt{2}}{2} \right) \end{aligned} \quad (10)$$



with suitable normalization $\langle \Psi_{1,2}^L | \Psi_{1,2}^R \rangle = \delta_{1,2}$. Finally, analytical forms of the group velocity $\mathbf{c}_g = \nabla \omega(\boldsymbol{\mu})$ for the above eigenstates can be easily deduced:

$$\mathbf{c}_g = \left(\frac{k_x d \sin \mu_x}{\sqrt{2m(k_x(1 - \cos \mu_x) + k_y(1 - \cos \mu_y))}}, \frac{k_y d \sin \mu_y}{\sqrt{2m(k_x(1 - \cos \mu_x) + k_y(1 - \cos \mu_y))}} \right) \quad (11)$$

where counter propagating states have opposite velocity sign $\mathbf{c}_{g,1,2} = \pm \mathbf{c}_g$. The direction of propagation ϕ follows:

$$\tan \phi(t) = \frac{c_{gy}}{c_{gx}} = \frac{k_y \sin \mu_y}{k_x \sin \mu_x}. \quad (12)$$

Interestingly, an incident state with arbitrary wavevector $\boldsymbol{\mu}$ propagates along the direction ϕ defined by the group velocity $\mathbf{c}_g(\boldsymbol{\mu})$, which is tailorable with $k_y(t)$. In other words, the analytical forms for $\omega_{1,2}$ and $\phi(\boldsymbol{\mu})$ delineate both frequency conversion and curvature of wave motion induced by the stiffness modulation which, in turn, can be tailored to functionally steer waves via adiabatic and nonadiabatic transformations.

We now discuss on the dynamics of smooth temporal modulations applied to the 2D lattice, and the relative transformation that takes place when an incident wave packet propagates in such a system. First and foremost, equation (9) have the same form of equation (3) and, as such, for any impinging wavevector $\boldsymbol{\mu}$, there are two counter propagating states that populate the lattice. It is straightforward to conclude that equation (5) can be employed to assess adiabaticity of the modulation, and gives the following condition for the velocity in order for a propagating state $|\psi_1^R\rangle e^{j\omega_1 t}$ not to leak energy toward $|\psi_2^R\rangle e^{j\omega_2 t}$:

$$|v_{\text{lim}}| \ll 16 \frac{\sqrt{\left(k_x \sin^2 \frac{\mu_x}{2} + k_y \sin^2 \frac{\mu_y}{2}\right)^3}}{\sqrt{m} \sin^2 \frac{\mu_y}{2}}. \quad (13)$$

In analogy to the procedure employed in the previous section, figure 4(c) illustrates the limiting condition for the speed of modulation to be considered adiabatic. This condition is valid for the entire wavenumber content of the incident wave packet, which consists of a prescribed displacement with central wavenumber $\boldsymbol{\mu} = [0.5\pi, 0.5\pi]$ and number of periods $n_x = n_y = 5$. To get to figure 4(c), the wavenumber dimension is eliminated by taking the minimum $\min_D \{v_{\text{lim}}(\boldsymbol{\mu}, t)\}$ and maximum $\max_D \{v_{\text{lim}}(\boldsymbol{\mu}, t)\}$ values within the domain $D = \mu_x \times \mu_y = [0.3\pi, 0.7\pi] \times [0.3\pi, 0.7\pi]$, which allowed us to include in the analysis all the relevant spectral content of the wavepacket.

Three distinct modulation velocities $v_1 = 93$, $v_2 = 10$, and $v_3 = 1.6$ are probed to qualify consistency of equation (13) and figure 4(c) via numerical simulation: it is expected that these values, defined across the limiting condition, allow us to shed light on the energy leaks which manifests in time-modulated lattices with concurrent frequency conversion and wave steering. We firstly show dispersion relations and group velocity profiles in figure 5(a) for consecutive time instants t_i , $t_m = (t_i + t_f)/2$ and t_f . We focus our attention

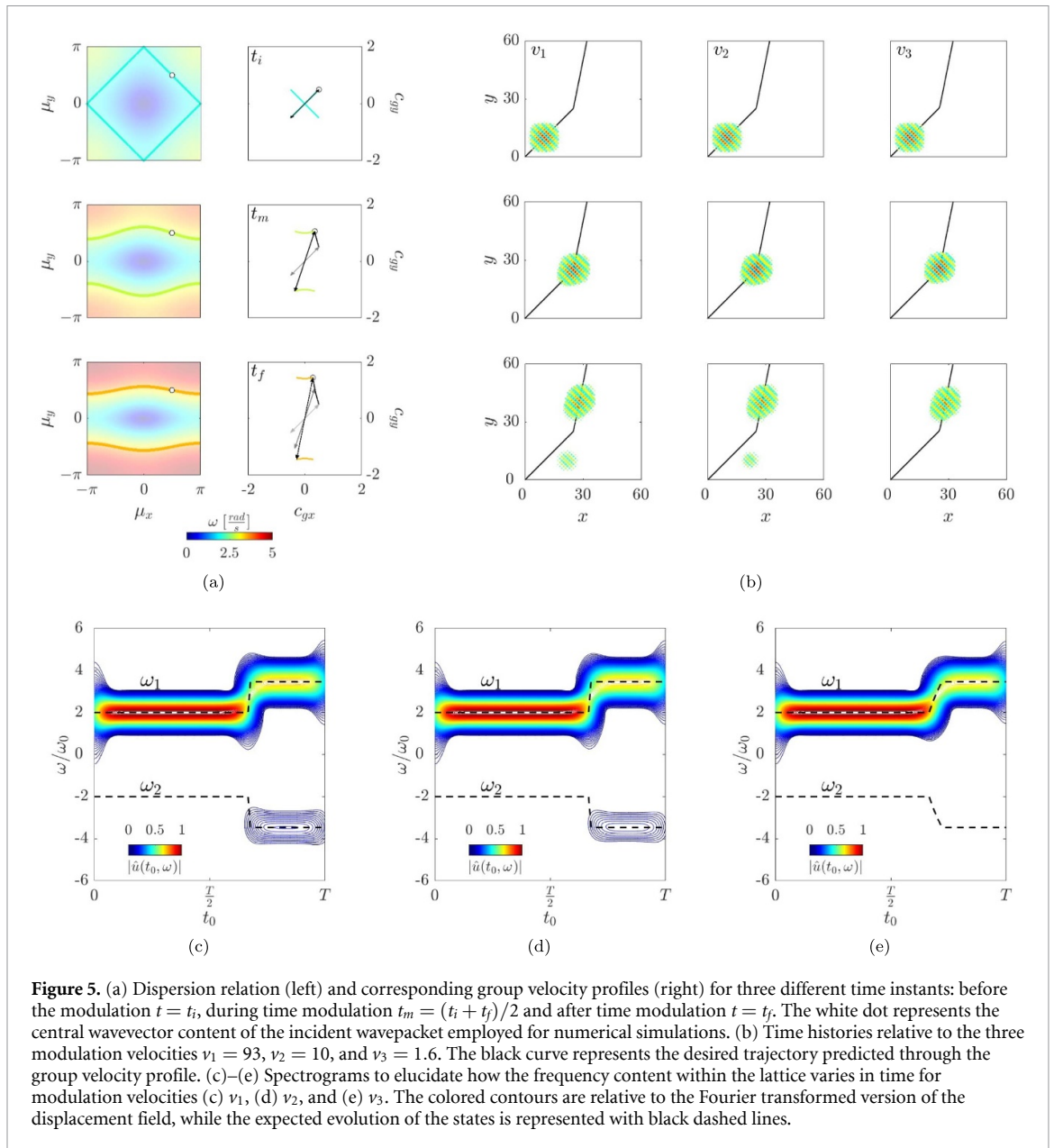
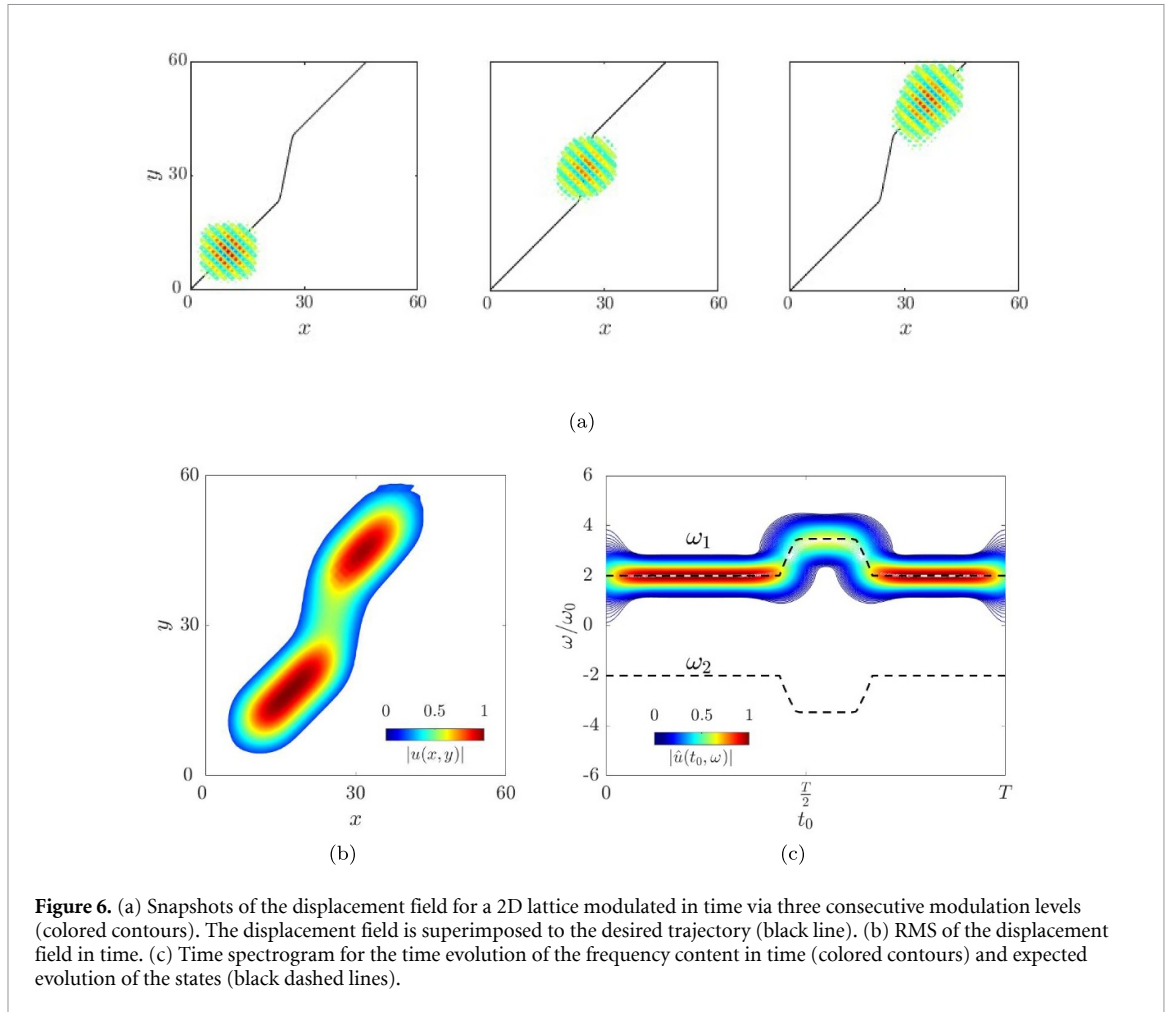


Figure 5. (a) Dispersion relation (left) and corresponding group velocity profiles (right) for three different time instants: before the modulation $t = t_i$, during time modulation $t_m = (t_i + t_f)/2$ and after time modulation $t = t_f$. The white dot represents the central wavevector content of the incident wavepacket employed for numerical simulations. (b) Time histories relative to the three modulation velocities $v_1 = 93$, $v_2 = 10$, and $v_3 = 1.6$. The black curve represents the desired trajectory predicted through the group velocity profile. (c)–(e) Spectrograms to elucidate how the frequency content within the lattice varies in time for modulation velocities (c) v_1 , (d) v_2 , and (e) v_3 . The colored contours are relative to the Fourier transformed version of the displacement field, while the expected evolution of the states is represented with black dashed lines.

on the central wavevector content $\mu = (0.5\pi, 0.5\pi)$ of the incident wave packet (highlighted with a white dot in the dispersion diagram). For such a point in reciprocal space, the corresponding group velocities are reported alongside the dispersion, with emphasis on how the directionality evolves over time. It is expected that the temporal evolution of a narrowband wavepacket does follow the directionality dictated by 5(a). Results from time simulations follow.

Three relevant snapshots prior, during, and after the modulation are illustrated in figure 5(b) for the three aforementioned modulation velocities. For comparison, the expected trajectory is predicted from integration of the group velocities in time and displayed in black underneath the displacement fields. We observe that all configurations are capable of curving the wave packet by the desired angle $\Delta\phi$ and, hence, are consistent with the group velocities illustrated in figure 5(a). In case of fast modulation v_1 , there is a relevant wave packet that separates from the incident state ω_1 , which is blueprint of energy leak across the temporal discontinuity. The reflected wave packet effectively embodies the energy transferred to state ω_2 via non-adiabatic passage, and propagates with opposite direction as compared to ω_1 . To decrease the energy leak, a sufficiently slow velocity v is to be employed. Configurations with $v = v_2$ and $v = v_3$ exhibit greater degree of adiabaticity and, hence, the reflection is minimal or absent. Animations are reported in the supplementary material.

To further verify the above considerations, the frequency spectrograms relative to the time histories are displayed in figures 5 (c)–(e). In analogy to 1D lattices, the wavenumber domain is eliminated by taking the



L^2 norm limited to $\mu_x > 0$ and $\mu_y > 0$. The results are consistent with the theory: fast and intermediate modulations (see figures 5(c) and (d)) are not adiabatic and, as such, there is energy transfer from the positive toward the negative frequencies. In contrast, sufficiently slow modulations (figure 5(e)) induce adiabatic transformations whereby the energy content represented in reciprocal space does not leave the incident state. Hence, in physical space, the trajectory of an incident wave-packet can be curved with minimal reflections.

Finally, we design a more complex adiabatic law for k_y , which consists of three consecutive stiffness levels $k_y = 1$, $k_y = 10$, and back to $k_y = 1$. Figure 6(a) illustrates temporal snapshots of the wave packet that, due to stiffness modulation, is capable of steering at will (animations are reported in the supplementary material). The curvature of wave motion is further highlighted by taking the *RMS* along the temporal dimension (figure 6(b)), whereby the lower amplitude in the central part is attributed both to a lower amplitude of wave motion and greater velocity of propagation. To conclude the paper, we demonstrate adiabaticity of this transformation which, according to the spectrogram in figure 6(c) occurs with negligible energy scattering toward counter-propagating states.

4. conclusions

In this paper, we explored the dynamics of slow temporal modulations in the context of mechanical waveguides. Wave motion in such systems is driven by the time-evolution of the underlying dispersion properties which, under quasi-static conditions, dictate both frequency conversion and directionality of wave motion. By way of the adiabatic theorem, we define a condition in order for the transformation to occur with negligible energy leakage, which is responsible for undesired reflections between wave modes that populate the waveguide. The concept is general and easily applicable to more complex scenarios. For example, in physical systems with tunable dispersion relations, such as beams with piezoelectric materials in mechanics [38, 46], and materials with tunable permittivity [48]. Although based on a very different phenomenon, we herein propose a waveguiding mechanism that allows an elastic signal to be sent from an emitter to a receiver, similarly (but conceptually very different) to what has been observed in many studies concerning quantum

valley Hall and quantum spin Hall-based waveguides. Future works will focus on the experimental analysis of 1D and 2D continuum phononic waveguides with time dependent elasticity.

Data availability statement

No new data were created or analysed in this study.

Appendix. Derivation of the limiting condition for adiabaticity

Consider the evolution equation equation (3) which describes wave motion for an impinging wave $|\hat{\Psi}_n\rangle = |\psi_1^R\rangle e^{j\omega_1 t}$ with incident wavenumber μ and unitary amplitude at $t = 0$. When the temporal modulation is turned on, the solution is synthesized through a linear combination of all the available wave modes $|\hat{\Psi}_n\rangle = \sum_{h=1}^2 a_h |\psi_h^R\rangle e^{j\theta_h}$ with participation factors a_h and geometric phase $\theta_h = \int_0^t \omega_h(\tau) d\tau$, whereby the frequencies ω_h and eigenvectors $|\psi_h^R\rangle$ are dictated by the quasi-static eigenvalue problem $H(\mu, t) |\psi_h^R\rangle = j\omega_h |\psi_h^R\rangle$. The substitution of the Ansatz $|\hat{\Psi}_n\rangle$ into equation (3) gives:

$$\sum_h (|\psi_{h,t}^R\rangle a_h + |\psi_h^R\rangle a_{h,t} + j\omega_h |\psi_h^R\rangle a_h) e^{j\theta_h} = H \sum_h |\psi_h^R\rangle a_h e^{j\theta_h} \quad (\text{A1})$$

which, due to the quasi-static eigenvalue problem, can be simplified as:

$$\sum_h (|\psi_{h,t}^R\rangle a_h + |\psi_h^R\rangle a_{h,t}) e^{j\theta_h} = 0. \quad (\text{A2})$$

Now, each side is left-multiplied by $\langle \psi_r^L |$ and the orthogonality of the eigenmodes $\langle \psi_r^L | \psi_h^R \rangle = \delta_{rh}$ is exploited to get to:

$$a_{r,t} = -\langle \psi_r^L | \psi_{r,t}^R \rangle a_r - \sum_{h \neq r} \langle \psi_r^L | \psi_{h,t}^R \rangle e^{j(\theta_h - \theta_r)} \quad (\text{A3})$$

which can be further expanded by differentiating the quasi-static eigenvalue problem $H |\psi_h^R\rangle = j\omega_h |\psi_h^R\rangle$

$$H_{,t} |\psi_h^R\rangle + H |\psi_{h,t}^R\rangle = j\omega_{h,t} |\psi_h^R\rangle + j\omega_h |\psi_{h,t}^R\rangle. \quad (\text{A4})$$

Left multiplying by $\langle \psi_r^L |$ and combining it with $\langle \psi_r^L | H |\psi_{h,t}^R\rangle = \langle \psi_r^L | \psi_{h,t}^R \rangle j\omega_r$

$$\begin{aligned} \langle \psi_r^L | H_{,t} |\psi_h^R\rangle + \langle \psi_r^L | H |\psi_{h,t}^R\rangle &= j\omega_{h,t} \langle \psi_r^L | \psi_h^R \rangle + j\omega_h \langle \psi_r^L | \psi_{h,t}^R \rangle \\ \langle \psi_r^L | H |\psi_{h,t}^R\rangle &= j\omega_r \langle \psi_r^L | \psi_{h,t}^R \rangle \end{aligned} \quad (\text{A5})$$

for $h \neq r$:

$$\langle \psi_r^L | H_{,t} |\psi_h^R\rangle = j(\omega_h - \omega_r) \langle \psi_r^L | \psi_{h,t}^R \rangle \quad (\text{A6})$$

which is substituted into equation (A3) to get to equation (4), discussed in the main text:

$$a_{r,t} = -\langle \psi_r^L | \psi_{r,t}^R \rangle a_r - \sum_{h \neq r} \frac{\langle \psi_r^L | H_{,t} |\psi_h^R\rangle}{j(\omega_h - \omega_r)} a_h e^{j(\theta_h - \theta_r)} \quad (\text{A7})$$

note that the energy, initially stored in the r^{th} mode, leaks to the h^{th} neighboring mode if the integral:

$$\int_0^t \sum_{h \neq r} \frac{\langle \psi_r^L | H_{,\xi} |\psi_h^R\rangle}{j(\omega_h - \omega_r)} a_h e^{j(\theta_h - \theta_r)} d\xi \quad (\text{A8})$$

is not negligible. In contrast, when the integral is sufficiently small, the impinging wave does not couple with the other states populating the lattice. Integrating by parts:

$$\int_0^t \sum_{h \neq r} \frac{\langle \psi_r^L | H_{,\xi} | \psi_h^R \rangle}{j(\omega_h - \omega_r)} a_h e^{j(\theta_h - \theta_r)} d\xi = - \sum_{h \neq r} \frac{\langle \psi_r^L | H_{,\xi} | \psi_h^R \rangle}{(\omega_h - \omega_r)^2} a_h e^{j(\theta_h - \theta_r)} \Big|_0^t + \int_0^t \frac{d}{d\xi} \left(\sum_{h \neq r} \frac{\langle \psi_r^L | H_{,\xi} | \psi_h^R \rangle}{(\omega_h - \omega_r)^2} a_h e^{j(\theta_h - \theta_r)} \right) d\xi \quad (\text{A9})$$

it can be shown that the higher order integral on the right hand side is small and therefore can be neglected [41]. For adiabaticity we require that:

$$\left| \frac{\langle \psi_h^L | H_{,t} | \psi_r^R \rangle}{(\omega_h - \omega_r)^2} \right| \ll 1 \quad (\text{A10})$$

which is the expression reported in equation (5) for $r = 1$ and $h = 2$ and employed in the paper to quantify the adiabaticity of time-modulated lattices.

ORCID iDs

Jonatha Santini  <https://orcid.org/0000-0002-2093-1529>

Emanuele Riva  <https://orcid.org/0000-0001-6773-9000>

References

- [1] Casadei F, Delpero T, Bergamini A, Ermanni P and Ruzzene M 2012 Piezoelectric resonator arrays for tunable acoustic waveguides and metamaterials *J. Appl. Phys.* **112** 064902
- [2] Wang P, Lu L and Bertoldi K 2015 Topological phononic crystals with one-way elastic edge waves *Phys. Rev. Lett.* **115** 104302
- [3] Huber S D 2016 Topological mechanics *Nat. Phys.* **12** 621
- [4] Miniaci M, Pal R, Morvan B and Ruzzene M 2018 Experimental observation of topologically protected helical edge modes in patterned elastic plates *Phys. Rev. X* **8** 031074
- [5] Pal R K and Ruzzene M 2017 Edge waves in plates with resonators: an elastic analogue of the quantum valley hall effect *New J. Phys.* **19** 025001
- [6] Riva E, Quadrelli D, Cazzulani G and Braghin F 2018 Tunable in-plane topologically protected edge waves in continuum kagome lattices *J. Appl. Phys.* **124** 164903
- [7] Qian K, Apigo D J, Prodan C, Barlas Y and Prodan E 2018 Topology of the valley-chern effect *Phys. Rev. B* **98** 155138
- [8] Jin Y, Torrent D and Djafari-Rouhani B 2018 Robustness of conventional and topologically protected edge states in phononic crystal plates *Phys. Rev. B* **98** 054307
- [9] Liu T-W and Semperlotti F 2018 Tunable acoustic valley-hall edge states in reconfigurable phononic elastic waveguides *Phys. Rev. Appl.* **9** 014001
- [10] Riva E, Rosa M I and Ruzzene M 2020 Edge states and topological pumping in stiffness-modulated elastic plates *Phys. Rev. B* **101** 094307
- [11] Kariyado T and Hatsugai Y 2015 Manipulation of dirac cones in mechanical graphene *Sci. Rep.* **5** 1
- [12] Wang Y-T, Luan P-G and Zhang S 2015 Coriolis force induced topological order for classical mechanical vibrations *New J. Phys.* **17** 073031
- [13] De Ponti J M, Iorio L, Riva E, Ardito R, Braghin F and Corigliano A 2021 Selective mode conversion and rainbow trapping via graded elastic waveguides *Phys. Rev. Appl.* **16** 034028
- [14] Alshaq M, Sugino C and Erturk A 2022 Programmable rainbow trapping and band-gap enhancement via spatial group-velocity tailoring in elastic metamaterials *Phys. Rev. Appl.* **17** L021003
- [15] Climente A, Torrent D and Sánchez-Dehesa J 2010 Sound focusing by gradient index sonic lenses *Appl. Phys. Lett.* **97** 104103
- [16] Tol S, Degertekin F L and Erturk A 2017 Phononic crystal luneburg lens for omnidirectional elastic wave focusing and energy harvesting *Appl. Phys. Lett.* **111** 013503
- [17] Allam A, Sabra K and Erturk A 2020 3D-printed gradient-index phononic crystal lens for underwater acoustic wave focusing *Phys. Rev. Appl.* **13** 064064
- [18] Zigoneanu L, Popa B-I and Cummer S A 2011 Design and measurements of a broadband two-dimensional acoustic lens *Phys. Rev. B* **84** 024305
- [19] Kim G, Portela C M, Celli P, Palermo A and Daraio C 2021 Poroelastic microlattices for underwater wave focusing *Extreme Mech. Lett.* **49** 101499
- [20] Chaplain G J, De Ponti J M, Aguzzi G, Colombi A and Craster R V 2020 Topological rainbow trapping for elastic energy harvesting in graded su-schrieffer-heeger systems *Phys. Rev. Appl.* **14** 054035
- [21] Skelton E, Craster R, Colombi A and Colquitt D 2018 The multi-physics metawedge: graded arrays on fluid-loaded elastic plates and the mechanical analogues of rainbow trapping and mode conversion *New J. Phys.* **20** 053017
- [22] Pendry J B, Schurig D and Smith D R 2006 Controlling electromagnetic fields *Science* **312** 1780
- [23] Leonhardt U 2006 Optical conformal mapping *Science* **312** 1777
- [24] Fleury R, Monticone F and Alù A 2015 Invisibility and cloaking: origins, present and future perspectives *Phys. Rev. Appl.* **4** 037001
- [25] Norris A N 2008 Acoustic cloaking theory *Proc. R. Soc. A* **464** 2411
- [26] Torrent D and Sánchez-Dehesa J 2008 Acoustic cloaking in two dimensions: a feasible approach *New J. Phys.* **10** 063015
- [27] Xu X, Wang C, Shou W, Du Z, Chen Y, Li B, Matusik W, Hussein N and Huang G 2020 Physical realization of elastic cloaking with a polar material *Phys. Rev. Lett.* **124** 114301
- [28] Chatzopoulos Z, Palermo A, Guenneau S and Marzani A 2022 Cloaking strategy for love waves *Extreme Mech. Lett.* **50** 101564

- [29] Quadrelli D E, Casieri M A, Cazzulani G, La Riviera S and Braghin F 2021 Experimental validation of a broadband pentamode elliptical-shaped cloak for underwater acoustics *Extreme Mech. Lett.* **49** 101526
- [30] Becker T S, Van Manen D-J, Haag T, Bärlocher C, Li X, Börsing N, Curtis A, Serra-Garcia M and Robertsson J O 2021 Broadband acoustic invisibility and illusions *Sci. Adv.* **7** eabi9627
- [31] Popa B-I, Zigoneanu L and Cummer S A 2011 Experimental acoustic ground cloak in air *Phys. Rev. Lett.* **106** 253901
- [32] Colombi A, Roux P, Guenneau S and Rupin M 2015 Directional cloaking of flexural waves in a plate with a locally resonant metamaterial *J. Acoust. Soc. Am.* **137** 1783
- [33] Nassar H, Yousefzadeh B, Fleury R, Ruzzene M, Alù A, Daraio C, Norris A N, Huang G and Haberman M R 2020 Nonreciprocity in acoustic and elastic materials *Nat. Rev. Mater.* **5** 667
- [34] Trainiti G and Ruzzene M 2016 Non-reciprocal elastic wave propagation in spatiotemporal periodic structures *New J. Phys.* **18** 083047
- [35] Riva E, Marconi J, Cazzulani G and Braghin F 2019 Generalized plane wave expansion method for non-reciprocal discretely modulated waveguides *J. Sound Vib.* **449** 172
- [36] Palermo A, Celli P, Yousefzadeh B, Daraio C and Marzani A 2020 Surface wave non-reciprocity via time-modulated metamaterials *J. Mech. Phys. Solids* **145** 104181
- [37] Park J and Min B 2021 Spatiotemporal plane wave expansion method for arbitrary space–time periodic photonic media *Opt. Lett.* **46** 484
- [38] Xia Y, Riva E, Rosa M I, Cazzulani G, Erturk A, Braghin F and Ruzzene M 2021 Experimental observation of temporal pumping in electromechanical waveguides *Phys. Rev. Lett.* **126** 095501
- [39] Grinberg I H, Lin M, Harris C, Benalcazar W A, Peterson C W, Hughes T L and Bahl G 2020 Robust temporal pumping in a magneto-mechanical topological insulator *Nat. Commun.* **11** 1
- [40] Riva E, Casieri V, Resta F and Braghin F 2020b Adiabatic pumping via avoided crossings in stiffness-modulated quasiperiodic beams *Phys. Rev. B* **102** 014305
- [41] Riva E, Castaldini G and Braghin F 2021 Adiabatic edge-to-edge transformations in time-modulated elastic lattices and non-hermitian shortcuts *New J. Phys.* **23** 093008
- [42] Chaunsali R, Li F and Yang J 2016 Stress wave isolation by purely mechanical topological phononic crystals *Sci. Rep.* **6** 30662
- [43] Yi K, Collet M and Karkar S 2017 Frequency conversion induced by time-space modulated media *Phys. Rev. B* **96** 104110
- [44] Trainiti G, Xia Y, Marconi J, Cazzulani G, Erturk A and Ruzzene M 2019 Time-periodic stiffness modulation in elastic metamaterials for selective wave filtering: theory and experiment *Phys. Rev. Lett.* **122** 124301
- [45] Pacheco-Pe na V and Engheta N 2020 Antireflection temporal coatings *Optica* **7** 323
- [46] Marconi J, Riva E, Di Ronco M, Cazzulani G, Braghin F and Ruzzene M 2020 Experimental observation of nonreciprocal band gaps in a space-time-modulated beam using a shunted piezoelectric array *Phys. Rev. Appl.* **13** 031001
- [47] Attarzadeh M, Callanan J and Nouh M 2020 Experimental observation of nonreciprocal waves in a resonant metamaterial beam *Phys. Rev. Appl.* **13** 021001
- [48] Pacheco-Pe na V and Engheta N 2020 Temporal aiming *Light Sci. Appl.* **9** 1